e-J. Surf. Sci. Nanotech. Vol. 1 (2003) 124-129 Conference - ALC '03 -

# Growth Morphologies and Defect Structure in Hexagonal Boron Nitride Films on Ni(111): A Combined STM and XPD Study *

Jürg Osterwalder,† Willi Auwärter, Matthias Muntwiler, and Thomas Greber
*Physik-Institut, Universität Zürich, Winterthurerstr.190, CH-8057 Zürich, Switzerland*
(Received 26 September 2003; Accepted 20 November 2003; Published 22 December 2003)

Well lattice-matched monolayer films of hexagonal boron nitride (*h*-BN) can be grown on Ni(111) surfaces, representing a nominally ideal interface for preparing ultimately thin metal-insulator-metal (MIM) structures. In a detailed study, combining local and non-local probes, the presence of characteristic defect lines is uncovered, and a model for their atomic structure is proposed. They have a strong influence on the growth morphologies of metal deposits. For room temperature deposition, they act as anchors for cluster nucleation, thus effectively short circuiting the MIM structure. For high-temperature deposition, the defects collect Co adatoms very efficiently and lead to Co intercalation underneath the *h*-BN film. [DOI: 10.1380/ejssnt.2003.124]

Keywords: Scanning Tunneling Microscopy; Photoelectron Diffraction Measurement; Surface Structure; Morphology, Roughness and Topography; Nickel; Boron Nitride; Cobalt; Single Crystal Epitaxy

## I. INTRODUCTION

Metal-insulator interfaces play a crucial role in many current and future electronic and spintronic devices. In view of the continuing reduction of the size of the building blocks, the abruptness of the transition from metallic to insulating regions is an important issue. For fundamental studies related to such transitions, an atomically sharp interface is a prerequisite. On Ni(111) a lattice-matched monolayer (ML) film of hexagonal boron nitride (*h*-BN) with (1x1) translational symmetry can be grown by high temperature decomposition of borazine $(HBNH)_3$ on the clean nickel surface [1], representing an ideal and prototypical case. This monolayer is insulating in the sense that the boron nitride bands appear at similar binding energies as in the bulk insulating phase and exhibit the same large 5 eV band gap [2,3]. Due to its well-defined monolayer thickness, the interface can be studied by scanning tunneling microscopy (STM) [4] and by angle-resolved photoemission spectroscopy (ARPES) [5].

In this paper we review a number of structural effects that have been observed on this interface, ranging from the geometric structure within the film and the registry with respect to the substrate, to the observation of linear defect lines and their interpretation in terms of boundaries of two almost degenerate but nevertheless different crystallographic domains. These defects cannot be completely avoided and represent an obstacle in the growth of metal-insulator-metal structures based on this ultimately thin *h*-BN layer, as is exemplified by the study of the Co deposits.

## II. EXPERIMENTAL

All the experiments described in this paper were carried out in an ultra-high vacuum system based on a Vacuum Generators ESCALAB 220 with a custom-made STM chamber and a transfer and preparation chamber attached to it. The cleaning procedure of the Ni(111) single crystal included cycles of 800 eV $Ar^+$ sputtering followed by annealing to 1000 K. In order to remove carbon contamination efficiently, the surface was occasionally exposed to 20 L (1 Langmuir = $10^{-6}$ torr seconds) of oxygen after sputtering. Monolayer and sub-monolayer films of *h*-BN were formed by exposing the surface to various doses of borazine $(HBNH)_3$ while the substrate was kept at 1070 K. After cooling down to room temperature, the films were characterized by low-energy electron diffraction (LEED) and by x-ray photoelectron spectroscopy (XPS). STM images were measured with a Park Scientific Instruments VPII STM using electrochemically etched tungsten tips. Using an in-vacuo sample goniometer [6], x-ray photoelectron diffraction data were recorded for both N 1s and B 1s signals excited by Si $K_\alpha$ radiation (1740 eV), as well as for Co 2p using Mg $K_\alpha$ radiation (1254 eV) in the case of Co deposits.

## III. RESULTS AND DISCUSSIONS

The growth of *h*-BN on Ni(111) is self-limiting at one monolayer. Once all nickel surface is covered, the reaction probability for arriving borazine molecules drops by orders of magnitude. Fig. 1a shows a large area STM image of such a completed monolayer. The film is extremely flat, with terrace widths of up to 2000 Å, and with no discernible vacancies or defects visible at this scale. The few steps in the image reflect steps of the underlying Ni(111) surface. On the terraces, the atomic lattice can be imaged at high resolution, suggesting the presence of a graphite-like *h*-BN sheet. The unit cell exhibits essentially three levels of gray scales. Very recently, Grad *et al.* [3] have used density functional theory (DFT) calculations in order to calculate local densities of states at a height of 2.5 Å above the *h*-BN monolayer. Their results permit to identify the bright spots with the positions of the N atoms while the B atoms are centered on the gray areas.

Already quite early, a structural model had been suggested for *h*-BN/Ni(111) on the basis of a quantitative LEED analysis by Gamou *et al.* [7]. It was found that N atoms occupy on-top positions, 2.22 Å above the Ni surface layer, and B atoms are located in *fcc* sites at a height

*This paper was presented at The 4th International Symposium on Atomic Level Characterizations for New Materials and Devices (ALC '03), Kauai, Hawaii, USA, 5-10 October, 2003.
†Corresponding author: osterwal@physik.unizh.ch

  

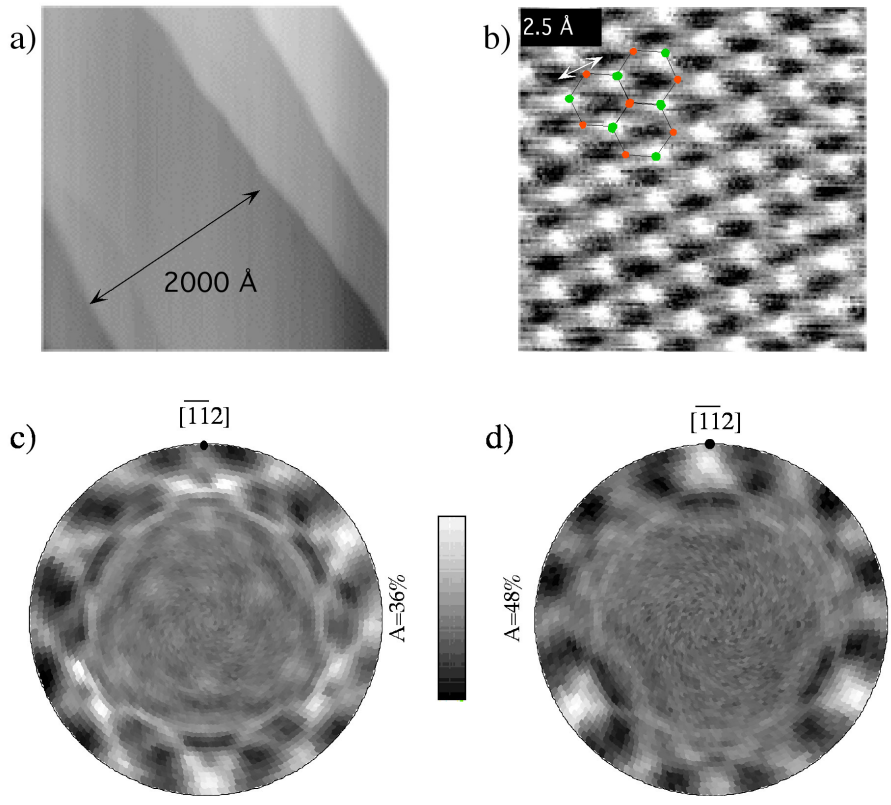


FIG. 1: (a) STM image of a complete *h*-BN monolayer on Ni(111) ($350 \times 350$ nm$^2$). It was taken in the constant current mode with a sample bias voltage $V_b$ of +100 mV and a tunneling current $I_t$ of 1 nA. (b) Atomic resolution image of the same layer ($1.6 \times 1.6$ nm$^2$), taken in constant height mode ($0.2 < I_t < 0.5$ nA) with $V_b$=+4.8 mV. A model atomic *h*-BN lattice is overlayed in one region of the image. (c) N 1s XPD pattern from a complete *h*-BN monolayer film ($E_{kin}$=1342 eV). N 1s photoemisson intensities are mapped over the complete emission hemisphere and represented in a linear gray scale and in stereographic projection. The full emission anisotropy A=($I_{max}$-$I_{min}$)/$I_{max}$ is indicated next to the gray bar. (d) Same, but for B 1s emission ($E_{kin}$=1550 eV) (from Ref. [4]).

of 2.04 Å. The *h*-BN layer appears to respond to the compressive strain due to small lattice mismatch (0.4%) with the nickel substrate by exhibiting this slight corrugation with an amplitude of 0.18 Å. This model is fully confirmed by the XPD data shown in Fig. 1c and d [4]. The absence of pronounced forward scattering signals near the center part of the XPD patterns (corresponding to high take-off angles) is a sensitive proof for the monolayer character of the film. Forward scattering peaks appear only near grazing emission along the rims of the patterns, together with well developed interference fringes. From the take-off angle of the three dominant forward scattering peaks in the B 1s emission pattern (Fig. 1d), an inclination angle of 4° can be deduced for the B-N bond. From the $(1 \times 1)$ in-plane registry with the Ni(111) substrate the in-plane lattice constant of the film is known and thence a corrugation of 0.1Å is concluded which is in agreement with results from DFT calculations [3], but somewhat less than the result from LEED [7]. More significant for what follows is the clear three-fold symmetry of the two patterns, which is consistent with the assignment (N,B) = (top,*fcc*) of the adsorption sites in the LEED study. Due to the weak backscattering amplitude for these adsorbate photoelectrons from the underlying Ni layers, the patterns do not contain the information on the adsorption sites. In a novel approach to use XPD data for adsorbate structure determination, Muntwiler *et al.* [8] have used Ni 2p substrate emission patterns from the clean and *h*-BN covered Ni(111) surface. From the observed weak differences the LEED result could be confirmed but with a slight refinement of the N-Ni bond distance (1.95 Å) for the on-top site. In any case, both these studies have identified a single crystallographic phase with unique adsorption sites for both N (on-top) and B (*fcc*) atoms.

As is so often the case, STM images permitting the observation of local geometries have revealed occasional defects in the films. These defects form straight lines and can extend over dozens of nanometers. They were found to influence the growth morphology of Co deposits on monolayer *h*-BN films [9] (see below), and an in-depth investigation of their character and their origin was thus carried out.

The key to solve this problem was found in the study of submonolayer film coverages [10]. In Fig. 2a the relevant part of the B 1s XPD pattern from a 0.25 ML *h*-BN film, containing the characteristic B-N forward scattering peaks along the [$\bar{1}$12] and equivalent directions (cf. Fig. 1d), is depicted. The pattern has been plotted in the same absolute orientation as the STM image of Fig. 2b, which is a conductance (dI/dV) image of the same film. For ob-

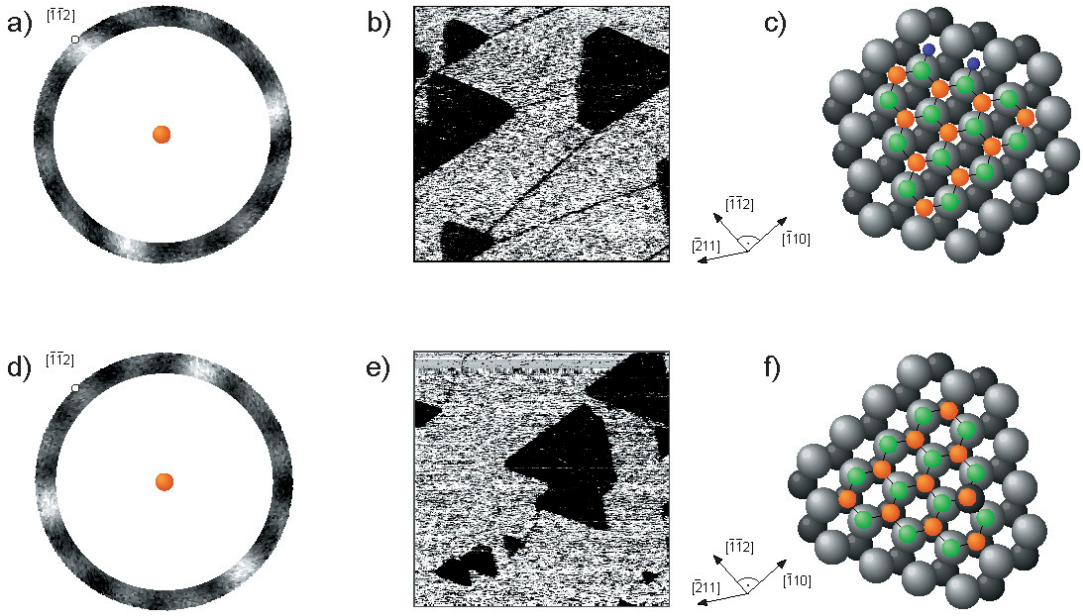


FIG. 2: XPD and STM data on submonolayer *h*-BN films exhibiting triangular islands. (a) and (d) represent Si $K_\alpha$ excited B 1s XPD patterns for polar angles $\theta$ from 78° to 86° and for two different film preparations resulting in predominantly one or the other type of crystallographic *h*-BN domain. (b) and (e) give STM conductance images ($400 \times 400$ nm$^2$, $V_b$ = -0.6 V, $I_t$ = 3 nA) for the same preparations, while (c) and (f) illustrate the structural models deduced from these data. First-layer (bright gray spheres) and second-layer (smaller, dark gray spheres) Ni atoms represent the Ni(111) surface. In (c) two hydrogen atoms (small blue spheres) indicate a possible hydrogen decoration of the island edges (from Ref. [10]).

taining this kind of image, the sample bias voltage $V_b$ was modulated with an amplitude of 40 meV at a frequency of 5 kHz and the current variations were detected by a lock-in amplifier. The low conductance of the *h*-BN film serves to identify directly the covered areas, while the exposed Ni(111) surface produces no contrast except along steps that appear as black lines. At this coverage, *h*-BN forms regular triangular islands of various sizes, but all oriented in the same way with one corner pointing along the $[\overline{11}2]$ direction. Combining the island shape and the crystallographic information one can draw the atomic model for a triangular island shown in Fig. 2c. In making the reasonable assumption that the boron nitride will tend to minimize the number of open bonds, the island boundaries are all nitrogen terminated. The single open bond per N atom may either be saturated by hydrogen atoms that cannot be detected, or by enhanced bonding of the island edges to the substrate.

Figs. 2d and e show corresponding data sets for a different preparation of a 0.2 ML film, where less care was taken to remove all carbon contamination from the Ni(111) surface prior to *h*-BN deposition. On this sample a substantial number of islands was observed that were oriented in the opposite way. At the same time the B-N forward scattering peaks in the B 1s XPD pattern appear at positions that are rotated by 60°, signaling a different crystallographic registry of the *h*-BN to the Ni(111) substrate. The atomic model for the triangular islands (Fig. 2f) illustrates the adsorption sites for this structure. It is known from DFT calculations [3] that there is a second structure that is almost degenerate to the lowest energy structure discussed so far. The N atoms are also in the on-top position, but the B atoms occupy *hcp* sites. This change accounts for the 60° rotation of the B-N bond observed in the XPD. Again, the island shape suggests that the edges are formed by N atoms. It appears that the presence of small amounts of carbon atoms, or other chemical or structural defects, leads to the nucleation of this second structure.

Wherever two islands of different domains meet, a straight line defect is detected in the STM images. Fig. 3a shows an area where both island types are found in fair numbers. At higher magnification (Fig. 3b) the line defects show up clearly where islands have coalesced. Based on this observation, and on the atomic models for the individual domains (Figs. 2c and f), one can deduce a detailed model for this structural defect, which is depicted in Fig. 3c. The defect is lined on either side by N atoms, and it represents a defect only in the boron sublattice, while the nitrogen sublattice runs continuously across.

In an attempt to prepare ultimately thin magnetic metal-insulator-metal junctions, small amounts of Co have been deposited on monolayer *h*-BN films [9]. A strong dependence of the growth morphology on the substrate temperature is observed. Room temperature (RT) deposition leads to drop-like three-dimensional (3D) islands (Fig. 4a). Upon closer inspection the islands, or clusters, often show a quasi-hexagonal footprint and a fairly narrow size distribution with diameters ranging from 2 to 3.5 nm and heights in the order of 0.4 to 0.8 nm, thus including between two and four atomic layers. A striking feature of the image in Fig. 4a is that the clusters are not randomly distributed over the surface. Many of the clusters arrange themselves to form linear chains of up to 100 nm length. The chain directions show a strong correlation with those crystal directions of the underlying

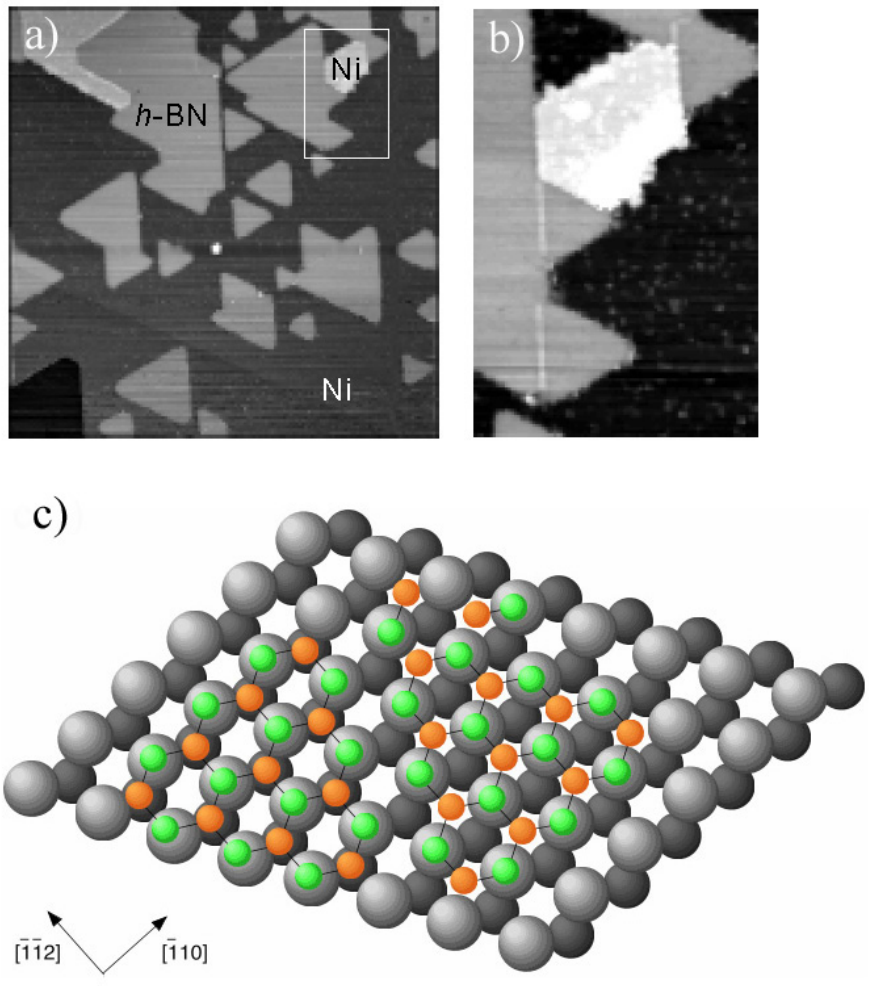


FIG. 3: (a) STM image for a submonolayer $h$-BN coverage of Ni(111) prepared under conditions such as to produce both types of island orientation ($310 \times 310$ nm$^2$, $V_b$ = -0.2 V, $I_t$ = 1 nA). (b) Enlarged image of the area marked in (a), using the same tunneling conditions. The bright patch in the upper half of the image represents a second Ni layer. (c) Atomic model of the defect forming along the line where two different domains meet (from Ref. [10]).

substrate along which the defect lines have been observed in the $h$-BN monolayers. Although it has not been possible to image a cluster chain and a line defect in the same image due to the strong difference in topographic variation, one can speculate that the linear defects act as anchors for cluster nucleation and are thus responsible for the chain formation. Similar cluster chains were also formed upon Cu deposition. The atomic model of the defect as depicted in Fig. 3c suggests that these anchors are provided by Co atoms located directly in *fcc* or *hcp* adsorption sites of the Ni(111) surface, forming a short circuit across the metal-insulator-metal structure.

For Co deposition on warm substrates (450 K), the STM images show predominantly two-dimensional (2D), one monolayer high, triangular islands (Fig. 4b). The island edges follow again the same crystallographic directions as the defect lines discussed above. Second and even third layer formation can be seen in some cases, but always preserving rather regular island shapes. Also here, the islands are not distributed uniformly over the surface but appear to be abundant in certain areas. Annealing the 3D clusters of a RT preparation does not produce this type of 2D clusters, indicating that kinetics play an important role during their formation. A very thorough analysis of all the available data, including STM, XPS and XPD, brought forward a picture where these 2D islands represent Co that has intercalated underneath the $h$-BN film, and where the defect lines again act as traps for diffusing Co atoms, permitting them to penetrate the film [9].

The first hint for this behavior came from XPD experiments. Neither B 1s nor N 1s emission patterns from $h$-BN films with Co deposits in the 0.2 ML coverage range (not shown) exhibit any signs of extra forward scattering peaks for low polar angles. The data for both RT and 450 K preparation look essentially like the patterns of Figs. 1c and d. For 3D clusters, this behavior is expected (cf. Fig. 5e); the B 1s and N 1s emission from the covered regions is sufficiently attenuated by the several layers of Co that their contribution to the overall signal, and thus to the measured diffraction pattern, can be neglected. On the other hand, for a surface covered to 20% by a monolayer thick Co layer, significant forward scattering peaks should appear in the patterns. A second hint came from STM tip

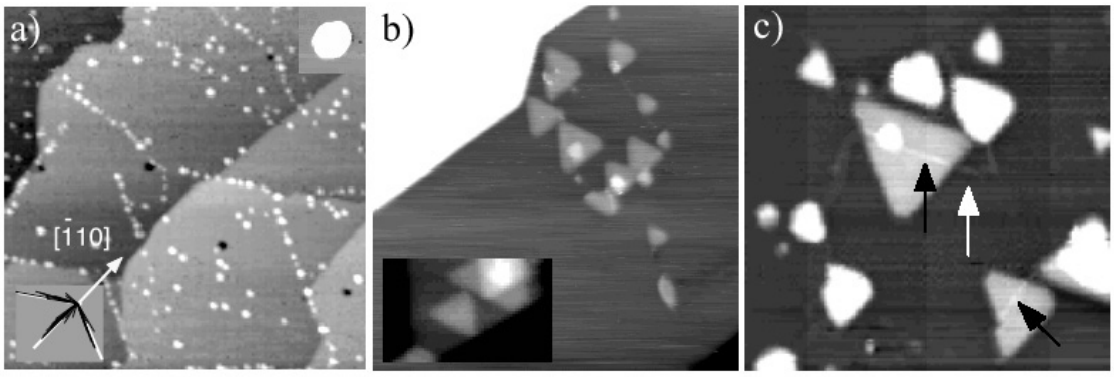


FIG. 4: STM images of Co deposits on *h*-BN/Ni(111). - (a) Co evaporation at room temperature ($105 \times 105$ nm$^2$, $V_b$ = -0.8 V, $I_t$ = 0.5 nA). The inset in the upper right corner illustrates the quasi-hexagonal cluster shape. In the bottom left inset, black lines represent the directions of cluster chains, while white lines indicate the crystal directions. (b) Co evaporation on the substrate kept at 450 K ($100 \times 100$ nm$^2$, $V_b$ = 0.06 V, $I_t$ = 1 nA). The inset highlights a region with Co growth over more than one monolayer. (c) Co evaporation at 450 K ($43 \times 43$ nm$^2$, $V_b$ = -0.1 V, $I_t$ = 2 nA), illustrating how defect lines (indicated by arrows) cross the monolayer-high Co islands (from Ref. [9]).

manipulation experiments. On a surface that exhibited a mixture of 3D and 2D islands, the tip could be placed over a 3D island, and the island could be removed from the surface by applying a voltage pulse. This suggests that the 3D islands represent nanosize metal-insulator-metal interfaces with a weak bonding of the islands to the underlying boron nitride. The same procedure did not work for 2D islands, indicating a much stronger bonding to the substrate.

In a systematic XPS study, the Co coverage versus exposure curves were measured for various temperatures [9]. It was found, that the sticking probability s for Co arriving on the film decreases over one order of magnitude in the temperature range from 200 K (s = 0.5) to 575 K (s = 0.05). The attenuation of the N 1s signal as a function of Co coverage is strongly reduced at elevated temperatures where the 2D islands are formed. This is clear evidence for *h*-BN remaining at the surface, effectively floating on top of the 2D Co islands.

In the STM images the 2D islands are often found crossing a defect line. This is illustrated in Fig. 4c, where the defect is actually seen both to the right of the island and on top of the island. If the defect line can be taken as a characteristic of the *h*-BN film, this is maybe the most direct evidence for the intercalation scenario. Furthermore, this correlation between defects and 2D islands supports a kinetic model for the formation of intercalated islands. The long linear extension of the defects makes their cross section for the attachment of diffusing Co adatoms very large. Once attached to the defect, they can easily bond to the Ni substrate on the exposed *hcp* or *fcc* sites (cf. model in Fig. 3c). In view of the low surface energy of the *h*-BN film, this is the energetically more stable site for Co. Due to the relatively weak bonding of the boron nitride to the Ni(111) surface, the film can apparently be lifted enough to accommodate the forming Co island underneath a *h*-BN carpet.

The Co 2p XPD data (Fig. 5) are less clear with respect to the intercalation model. The experimental patterns for RT and for 450 K preparation (Figs. 5a and b) are rather similar, in spite of the strongly different morphologies seen in the STM images. The high-temperature preparation exposes forward scattering peaks that can be well explained by a double layer of Co sitting on top of a *h*-BN layer (Fig. 5c, red dots), except for the peak in the center of the pattern. A third layer (Fig. 5c, blue dots) does not fit the data. On the other hand, the dot pattern overlayed in Fig. 5d, representing forward scattering directions for Co emisson through a *h*-BN cover, provides a fairly good match to the measured forward scattering pattern. Unfortunately, the two growth scenarios (Fig. 5e) produce patterns that are too similar to provide a clear discrimination.

## IV. CONCLUSIONS

This work exemplifies the characterization of an ' ideal ' metal-insulator-metal junction at the atomic level by a combination of STM images and spatially averaging XPS and XPD data. Most notable is the discovery of defect lines and their correlation with the presence of two distinct crystallographic registries of the *h*-BN with respect to the Ni(111) surface layer. From this, a model for the atomic structure at the defect could be constructed. Moreover, the importance of the defect in defining the growth morphology of Co deposits is demonstrated, making this junction far less ideal than previously expected. This kind of detailed interface study is thus very important in order to learn the behavior of materials when forming devices on a nanometer scale.

### Acknowledgments

We are grateful to H. Sachdev for providing us the borazine, to P. Blaha and G. Grad for giving us invaluable theoretical input for our data interpretation, and to F. Baumberger, A. Tamai, M. Corso, W. Deichmann and M. Klöckner for help with the experiments. This work was supported by the Swiss National Science Foundation.

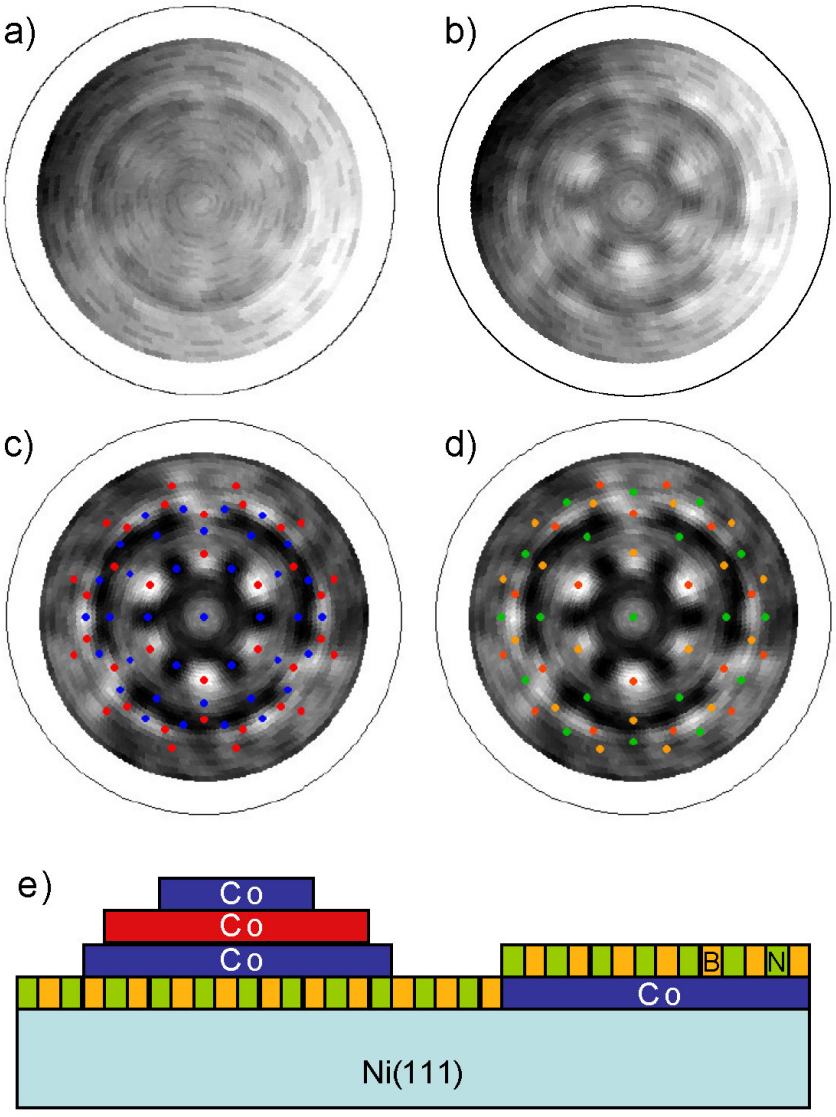


FIG. 5: Co 2p XPD data (Mg K$\alpha$, $E_{kin}$ = 475 eV) from Co deposits of 0.2 ML on $h$-BN/Ni(111). The orientation of the graphs is such that the [$\overline{1}$12] azimuth is pointing towards the top. (a) Co evaporation at room temperature, and (b) at 450 K. (c) The pattern of (b) after subtraction of a smooth, polar-angle dependent background, emphasizing the diffraction features in the data. The red (blue) dots overlayed on top of the data indicate forward scattering directions for Co emission from a first layer through Co scatterers in a second (third) layer. *hcp* stacking is assumed, with two different initial stacking sequences to provide a six-fold symmetric pattern. (d) Same as (c), but this time indicating forward scattering directions from a monolayer of Co emitters through a single layer of $h$-BN, including both domains (B in *fcc* (red) or *hcp* (yellow) sites), again producing a six-fold symmetric pattern. In (e) the two growth models are illustrated.

[1] A. Nagashima, N. Tejima, Y. Gamou, T. Kawai, C. Oshima, Phys. Rev. B **51**, 4606 (1995).
[2] A. Nagashima, N. Tejima, Y. Gamou, T. Kawai, C. Oshima, Phys. Rev. Lett. **75**, 3918 (1995).
[3] G. B. Grad, P. Blaha, K. Schwarz, W. Auwärter, T. Greber, Phys. Rev. B **68**, 085404 (2003).
[4] W. Auwärter, T. J. Kreutz, T. Greber, J. Osterwalder, Surf. Sci. **429**, 229 (1999).
[5] T. Greber, W. Auwärter, M. Hoesch, G. Grad, P. Blaha, J. Osterwalder, Surf. Rev. Lett. **9**, 1243 (2002).
[6] T. Greber, O. Raetzo, T. J. Kreutz, P. Schwaller, W. Deichmann, E. Wetli, J. Osterwalder, Rev. Sci. Instrum. **68**, 4549 (1997).
[7] Y. Gamou, M. Terai, A. Nagashima, C. Oshima, Sci. Rep. RITU A **44**, 211 (1997).
[8] M. Muntwiler, T. Greber, J. Osterwalder, Surf. Sci. **472**, 125 (2001).
[9] W. Auwärter, M. Muntwiler, T. Greber, J. Osterwalder, Surf. Sci. **511**, 379 (2002).
[10] W. Auwärter, M. Muntwiler, J. Osterwalder, T. Greber, Surf. Sci. Lett. **545**, L735 (2003).